Self-Tuning State-Feedback Control of Rotary Pendulum via Online Adaptive Reconfiguration of Control Penalty-Factor

Omer Saleem[1], Khalid Mahmood-ul-Hasan[2], Mohsin Rizwan[3]

[1]Department of Electrical Engineering, National University of Computer and Emerging Sciences, Lahore, Pakistan (e-mail: omer.saleem@nu.edu.pk)
[2]Department of Electrical Engineering, University of Engineering and Technology, Lahore, Pakistan (e-mail: kmhasan@uet.edu.pk)
[3]Department of Mechatronics and Control Engineering, University of Engineering and Technology, Lahore, Pakistan (e-mail: mohsin.rizwan@uet.edu.pk)

Abstract: This paper presents an online self-tuning state-feedback controller for under-actuated systems in order to enhance the system's position-regulation accuracy, disturbance-rejection capability and control input efficiency. The Linear-Quadratic-Regulator (LQR) is employed as the baseline state-feedback controller whose gains are dynamically reconfigured by adaptively modulating the control penalty-factor associated with the quadratic performance-criterion associated with the controller. The main contribution of this article is the methodical formulation of an original reconfiguration block that dynamically adjusts the control penalty-factor via a self-regulating secant-hyperbolic function to flexibly manipulate the control procedure while maintaining its asymptotic-stability. The proposed reconfiguration strategy modifies the control penalty-factor online with respect to the state-error feedback as well as the control-input dynamics. The benefits afforded by the proposed self-tuning controller are verified by conducting hardware-in-the-loop experiments on the QNET 2.0 Rotary Pendulum board. The experimental results show that the proposed strategy renders rapid transits with strong damping against parametric uncertainties in pendulum's body-angle responses, while limiting the peak servo requirements of the actuator.

Keywords: Linear quadratic regulator, self-tuning control, control penalty-factor, online reconfiguration, nonlinear scaling functions, rotary inverted pendulum.

1. INTRODUCTION

The under-actuated electro-mechanical systems are an essential component of robotic systems, precision manufacturing machines, biomedical implants, and aerospace applications, etc (Mahmoud, 2018). However, with the rapid advancement in technology, synthesizing robust-optimal controlling tools for such complex dynamical systems has posed a great challenge (An-chyau et al., 2015; Szuster and Hendzel, 2017). The ubiquitous state-feedback controllers, such as Linear-Quadratic-Regulator (LQR) and its modified variants, are widely favored to optimally control the under-actuated systems with nonlinear dynamics (Shahab et al., 2017). They yield optimal control decisions by minimizing a Quadratic-Performance-Index (QPI) that captures the real-time variations in state dynamics and control input of the system, while upholding the asymptotic stability throughout the operating regime (Saleem and Rizwan, 2019). These attributes make them superior to other model-free classical compensators, such as the PID controllers (Bhatti et al., 2015), the sliding mode controllers (Ullah et al., 2019), fuzzy-logic controllers (Saleem et al., 2017), and neural controllers (Saleem et al., 2019a), etc. The aforementioned classical control solutions are generally avoided owing to their inherent structural limitations, lack of sufficient stability proof, offline tuning of a multitude of parameters, induction of chattering in the response, empirical selection of logical rules, and requirement of extensive training data (Saleem et al., 2018a; Bhatti et al., 2018). However, despite its optimal behavior, even the LQR lacks robustness against modeling uncertainties, identification errors, and random parametric variations (Prasad et al., 2014; Ghartemani et al., 2011). The robust controllers, such as LMI and H_∞ systems, put unnecessary restraints on deriving the exact solution due to the boundary conditions and complex geometry of the system (Yang and Zheng, 2018).

The robustness of state-feedback controllers against parametric uncertainties can be enhanced by augmenting them with a well-postulated stable self-tuning adaptive system [Saleem et al., 2018b; Saleem et al., 2019b; Ning et al., 2019]. The conventional Model-Predictive-Controllers (MPCs) optimize the system in a receding horizon and solve the optimization problem in smaller time frames, which leads to new but sub-optimal solutions (Önkol and Kasnakoğlu, 2018). However, an ill-postulated MPC leads to wrong predictions which results in fragile control effort under long drifting disturbances (Bavili et al., 2015). The Model-Reference-Adaptive-Controller is synthesized by retrofitting the state-space controller with a stable online gain-adjustment law (Kavuran et al., 2017). Despite its guaranteed Lyapunov-stability, the selection of adaptation-rates is a cumbersome process (Saleem et al., 2020). The adaptive control laws synthesized via State-Dependent-Riccati-Equation are widely used to regulate the open-loop unstable and highly-nonlinear systems (Batmani et al., 2017). Deriving accurate state-dependent coefficient matrices to fully realize nonlinear characteristics of the system is extremely difficult due to the system's complex dynamics (Nekoo and Geranmehr, 2014). The indirect adaptive control scheme, equipped with self-adjusting state penalty-factors of QPI, has yielded promising results for under-actuated systems (Zhnag et al., 2014). Despite offering enhanced degree-of-freedom, defining unique set of analytical or logical rules to alter each state penalty-factor becomes drastically hectic, especially, if the system has a large number of state-variables (Basua and Nagarajaiaha, 2008). A practicable self-tuning strategy has been proposed in (Filip et al., 2020) that enhances the robustness of minimum variance controller for induction generators, via discrete settings of control penalty-factor across different operating conditions.

This paper presents the systematic development of a simple yet robust self-tuning state-feedback control strategy for the under-actuated electro-mechanical systems by adaptively reconfiguring the control penalty-factor associated with the controller's QPI. The proposed approach is beneficial because the control penalty-factor decisively steers the control-input trajectory which directly influences the robustness and control-efficiency of the system. Hence, the novel contribution of this paper is the formulation of a stable online reconfiguration block that is retrofitted with the baseline fixed-gain LQR to automatically self-adjust the control penalty-factor of its QPI by using a self-regulating continuous nonlinear scaling function. This arrangement dynamically alters the solution of Matrix-Riccati-Equation after every sampling interval, to online adapt the state-feedback gains. The proposed reconfiguration block constitutes a decaying Hyperbolic-Secant-Function (HSF) that is driven by the weighted sum of state-error variables. The continuity of HSF offers smooth gain transition across the entire operating regime. Additionally, the variation-rate of the HSF is dynamically self-regulated with respect to the variations in control-input. This feature flexibly manipulates the control procedure to effectively compensate the exogenous disturbances, while maintaining the control-input economy and asymptotic-convergence. The efficacy of the proposed adaptive controller is validated by conducting credible hardware-in-the-loop experiments of QNET 2.0 Rotary Pendulum board. The rotary pendulum system is selected owing to its under-actuated nature and open-loop unstable behavior. The experimental results clearly show that the proposed adaptive controller enhances the system's disturbance-rejection capability while effectively limiting the overall control energy expenditure.

There has been no significant contribution in the open literature to indirectly self-tune the state-feedback gains of LQR by adaptively tuning the control penalty-factor as a continuous nonlinear function of system's observable state-dynamics, in order to stabilize an under-actuated mechatronic system. Hence, this paper mainly focuses on exploring and validating the aforementioned idea.

The remaining paper is structured as follows. The mathematical model of the system is presented in Section 2. The baseline state-feedback controller is discussed in Section 3. The design procedure of the proposed self-tuning regulator is presented in Section 4. The reconfiguration blocks are formulated in Section 5. The experimental evaluation procedure and the results are illustrated in Section 6. The paper is concluded in Section 7.

2. SYSTEM MODELING

The Rotary-Inverted-Pendulum (RIP) is an inherently unstable and nonlinear dynamical system that is widely used as a standard benchmark to test the efficacy of control algorithms for under-actuated multivariable systems (Shahab et al., 2017). The inverted pendulum theory is considered as a core component in designing stabilization control strategies for higher-order complex mechatronic systems (Boubaker and Iriarte, 2017). The aforementioned attributes makes the RIP system an ideal candidate to validate the robustness of the proposed adaptive control scheme in this research. A simplified hardware schema of the RIP system is shown in Fig. 1. The postural stability of the pendulum is maintained via a single permanent magnet DC geared-motor that is actuated by applying the control input voltage, V_m, to its terminals. The DC motor shaft is coupled to the pendulum's arm in order to rotate it about the z-axis. The angular-displacement of the arm is denoted as θ. The arm's rotation energizes the pendulum's rod to uphold its vertical stability. The angular-displacement of the rod is denoted as θ. The state-space model of a linear system is given by (1) and (2).

$$\dot{x}(t) = \boldsymbol{A}x(t) + \boldsymbol{B}u(t) \tag{1}$$

$$y(t) = \boldsymbol{C}x(t) + \boldsymbol{D}u(t) \tag{2}$$

where, x is the state-vector, y is the output-vector, u is the control input signal, $\boldsymbol{A}$ is the state-transition matrix, $\boldsymbol{B}$ is the control-input matrix, $\boldsymbol{C}$ is the output matrix, and $\boldsymbol{D}$ is the feed-forward matrix. The state-vector and the control input-vector of the system are symbolically represented as follows (Saleem and Mahmood-ul-Hasan, 2019).

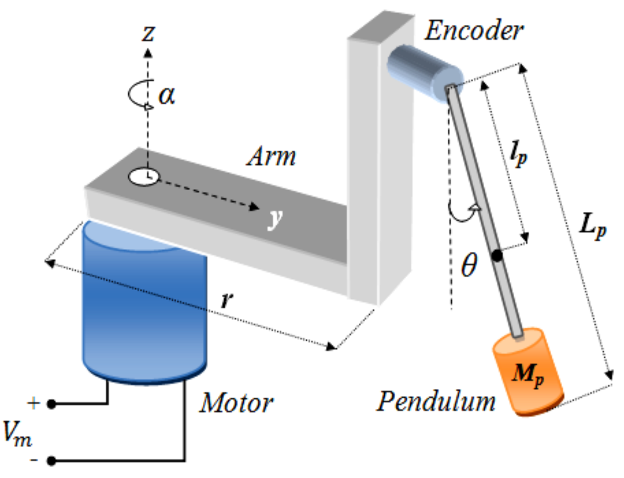

Fig. 1. Hardware diagram of the RIP systems

$$x = [\alpha \quad \theta \quad \dot{\alpha} \quad \dot{\theta}]^T, \qquad u = V_m \tag{3}$$

The nominal state-space model of the RIP system is defined in (4), (Saleem and Mahmood-ul-Hasan, 2019).

$$A = \begin{bmatrix} 0 & 0 & 1 & 0 \\ 0 & 0 & 0 & 1 \\ 0 & a_1 & a_2 & 0 \\ 0 & a_3 & a_4 & 0 \end{bmatrix}, \qquad B = \begin{bmatrix} 0 \\ 0 \\ b_1 \\ b_2 \end{bmatrix},$$

$$C = \begin{bmatrix} 1 & 0 & 0 & 0 \\ 0 & 1 & 0 & 0 \\ 0 & 0 & 1 & 0 \\ 0 & 0 & 0 & 1 \end{bmatrix}, \qquad D = \begin{bmatrix} 0 \\ 0 \\ 0 \\ 0 \end{bmatrix} \tag{4}$$

where,

$$a_1 = \frac{rM_p^2 l_p^2 g}{J_p J_e + J_e l_p^2 M_p + J_p M_p r^2}, a_2 = \frac{-K_t K_m (J_p + M_p l_p^2)}{(J_p J_e + J_e l_p^2 M_p + J_p M_p r^2) R_m},$$

$$a_3 = \frac{M_p l_p g (J_e + M_p r^2)}{J_p J_e + J_e l_p^2 M_p + J_p M_p r^2}, a_4 = \frac{-r M_p l_p K_t K_m}{(J_p J_e + J_e l_p^2 M_p + J_p M_p r^2) R_m},$$

$$b_1 = \frac{K_t (J_p + M_p l_p^2)}{(J_p J_e + J_e l_p^2 M_p + J_p M_p r^2) R_m}, b_2 = \frac{r M_p l_p K_t}{(J_p J_e + J_e l_p^2 M_p + J_p M_p r^2) R_m}$$

The modeling parameters of the RIP system, used in this research, are identified in Table 1 (Saleem and Mahmood-ul-Hasan, 2019).

3. PRIMARY STATE-FEEDBACK CONTROLLER

The LQR is an optimal state-feedback controller that has garnered a lot of traction owing to its capability of operating and controlling multivariable systems with minimum cost (Lewis et al., 2012). The fixed-gain LQR provides automated procedure to compute optimal control solutions by minimizing a QPI, given in (5), which captures the state-variations and control-input of the linear system (Saleem and Rizwan, 2019).

$$J_{lq} = \frac{1}{2}\int_0^\infty [x(t)^T \boldsymbol{Q} x(t) + u(t)^T \boldsymbol{R} u(t)]\, dt \tag{5}$$

Table 1. Modelling parameters of the RIP system

Parameter	Symbol	Value
Mass of pendulum	M_p	0.027 kg
Pendulum center of mass	l_p	0.153 m
Length of pendulum rod	L_p	0.191 m
Length of horizontal arm	r	0.083 m
Mass of arm	M_{arm}	0.028 kg
Gravitational acceleration	g	9.810 m/s^2
Moment about motor shaft	J_e	1.23×10^{-4} kgm^2
Moment about pendulum	J_p	1.10×10^{-4} kgm^2
Motor armature resistance	R_m	3.30 Ω
Motor armature inductance	L_m	47.0 mH
Motor torque constant	K_t	0.028 N.m
Back e.m.f. constant	K_m	0.028 V/(rad/s)
Maximum torque	T_m	0.14 Nm

where, $\boldsymbol{Q} \in \mathbb{R}^{4\times4}$ and $\boldsymbol{R} \in \mathbb{R}$ are the state- and control-penalty matrices, respectively. The selection of $\boldsymbol{Q}$ and $\boldsymbol{R}$ matrices are very important for robust stabilization of the RIP system [5]. In a sense, they are the figure-of-merit used to compute the optimal control solution. These matrices are selected such that, $\boldsymbol{Q}$ is a positive semi-definite matrix and $\boldsymbol{R}$ is a positive definite matrix. They are symbolically represented as follows.

$$\boldsymbol{Q} = diag(q_\alpha \quad q_\theta \quad q_{\dot{\alpha}} \quad q_{\dot{\theta}}), \quad \boldsymbol{R} = \rho \tag{6}$$

where, q_x and ρ represent the real-numbered penalty-factors of the $\boldsymbol{Q}$ and $\boldsymbol{R}$ matrices, respectively, and the subscript 'x' represents the corresponding state-variable. The value of ρ is selected as unity in this research to limit the peak actuating torques in the control profile while damping the overshoots. In this work, the $\boldsymbol{Q}$ matrix is empirically selected offline via trial-and-error by iteratively minimizing the cost-function shown in (7).

$$J_e = \int_0^\infty |e_\alpha(t)|^2 + |e_\theta(t)|^2 + |u(t)|^2\, dt \tag{7}$$

such that, $\quad e_\theta(t) = \pi - \theta(t), \quad e_\alpha(t) = \alpha_{ref} - \alpha(t)$

For position-regulation applications, the initial angular position of pendulum-arm is recorded at the beginning an experimental trial and is then used as its reference, α_{ref}. The selection of $\boldsymbol{Q}$ is done by applying a particular set of state penalty-factors to the LQR, observing the position-regulation behavior of the pendulum, and evaluating the cost using the function in (7). The state penalty-factors, shown in (8), yield the minimum cost and are thus chosen for this work.

$$\boldsymbol{Q} = diag(32.8 \quad 52.2 \quad 6.1 \quad 2.5), \quad \boldsymbol{R} = 1 \tag{8}$$

The selected $\boldsymbol{Q}$ and $\boldsymbol{R}$ matrices are then used to solve the Algebraic Riccati Equation (ARE). The solution of ARE is the symmetric positive definite matrix, $\boldsymbol{P}$, as shown in (9), (Saleem and Rizwan, 2019).

$$\boldsymbol{A}^T\boldsymbol{P} + \boldsymbol{P}\boldsymbol{A} - \boldsymbol{P}\boldsymbol{B}\boldsymbol{R}^{-1}\boldsymbol{B}^T\boldsymbol{P} + \boldsymbol{Q} = 0 \tag{9}$$

where, $\boldsymbol{P} \in \mathbb{R}^{4\times4}$. It is used to evaluate the state-feedback gain vector, $\boldsymbol{K}$, as shown in (10).

$$\boldsymbol{K} = \boldsymbol{R}^{-1}\boldsymbol{B}^T\boldsymbol{P} \tag{10}$$

If the system is controllable, the solution of ARE yields a stable and convergent control behavior (Lewis et al., 2012). This is a sufficient proof of stability for the proposed linear control law. The state-feedback gains evaluated offline in this research are $\boldsymbol{K} = [-6.21 \quad 130.56 \quad -4.22 \quad 17.83]$. Additionally, the linear control law in (10) is also retrofitted with the integral-of-error variables in α and θ. These auxiliary variables aid the system in damping the oscillations and improving its reference-tracking accuracy (Saleem et al., 2018b). The integral control law is given as follows.

$$u_i(t) = \boldsymbol{K}_i \varepsilon(t) = [K_{I\alpha} \quad K_{I\theta}] \begin{bmatrix} \varepsilon_\alpha(t) \\ \varepsilon_\theta(t) \end{bmatrix} \tag{11}$$

such that, $\varepsilon_\alpha(t) = \int_0^t e_\alpha(\tau)\, d\tau$, $\varepsilon_\theta(t) = \int_0^t e_\theta(\tau)\, d\tau$

The coefficients of integral gain vector, $\boldsymbol{K}_i$, are selected offline via trial-and-error by minimizing the cost-function, J_e, to attain best position regulation accuracy. The computed integral gains are $\boldsymbol{K}_i = [-2.06 \quad -7.47 \times 10^{-6}]$. The resulting fixed-gain LQR control law is expressed in (12).

$$u(t) = -\boldsymbol{K}x(t) + \boldsymbol{K}_i\varepsilon(t) \tag{12}$$

4. PROPOSED ADAPTIVE CONTROLLER DESIGN

In optimal regulator problems, the value of $\boldsymbol{R}$ directly manipulates the control input profile. The control penalty-factor weights the control-input variable in the QPI. The fixed value of control penalty-factor, ρ, makes a trade-off between the system's disturbance-rejection capability and its control-input requirements. This arrangement makes the control procedure wasteful in terms of available control resources. It unnecessarily applies more controlling force than required under small perturbations. Conversely, it contributes insufficient controlling force under large perturbations. Thus, it is imperative to dynamically adjust the value of ρ in LQR's QPI to attain robust controlling effort. This modification will effectively suppress the detrimental effects of the exogenous disturbances, while maintaining a reasonable control economy (Filip and Szeidert, 2017). It also obviates the requirement of empirically selecting the control penalty-factor via iterative tuning methods for different operating conditions. The dynamic adjustment of ρ is done via a pre-calibrated state-error dependent continuous nonlinear scaling function. The objective is to achieve a favorable balance between the system's control economy and disturbance-rejection capability. A detailed discussion regarding the online modification procedure of ρ, on the basis of the system's state-error feedback, is presented in the following section. With the proposed augmentation in place, the updated expression of QPI is given by (13).

$$J_{lq} = \frac{1}{2}\int_0^\infty [x(t)^T\boldsymbol{Q}x(t) + u(t)^T\boldsymbol{R}(t)u(t)]\, dt \tag{13}$$

The proposed adaptive framework uses the originally prescribed state-penalty matrix $\boldsymbol{Q}$, expressed in (8). However, the control penalty matrix is revised as follows.

$$\boldsymbol{Q} = diag(32.8 \quad 52.2 \quad 6.1 \quad 2.5), \qquad \boldsymbol{R}(t) = \rho(t) \tag{14}$$

where, $\rho(t)$ represents the time-varying control penalty-factor. In an infinite horizon control problem, this arrangement dynamically alters the solutions of the Matrix-Riccati-Equation as shown in (15).

$$\boldsymbol{A}^T\boldsymbol{P}(t) + \boldsymbol{P}(t)\boldsymbol{A} - \boldsymbol{PB}\big(\boldsymbol{R}(t)\big)^{-1}\boldsymbol{B}^T\boldsymbol{P} + \boldsymbol{Q} = 0 \tag{15}$$

where, $\boldsymbol{P}(t)$ is the time-varying solution of the ARE that is used as the input of the adjustable state-feedback gain vector, $\boldsymbol{K}(t)$, shown in (16).

$$\boldsymbol{K}(t) = \big(\boldsymbol{R}(t)\big)^{-1}\boldsymbol{B}^T\boldsymbol{P}(t) \tag{16}$$

The proposed self-tuning (reconfigurable) state-feedback control law is given by the following expression.

$$u(t) = -\boldsymbol{K}(t)x(t) + \boldsymbol{K}_i\varepsilon(t) \tag{17}$$

The coefficients of $\boldsymbol{K}_i$ are kept fixed at their originally prescribed values. The proposed adaptive controller is illustrated in Fig. 2. The proposed framework ensures an asymptotically-stable control behavior, if $\rho(t) > 0$.

5. RECONFIGURATION SCHEME FOR CONTROL PENALTY-FACTOR

The nominal state-feedback controller is augmented with a reconfiguration block to online adapt the value of ρ. This block redesigns the controller characteristics online in order to enhance the controller's adaptability and ensure optimum allocation of control resources under exogenous disturbances. This section presents two techniques for online modification of ρ. In both techniques, a pre-calibrated Hyperbolic-Secant-Function (HSF) is used to scale the value of ρ. The continuous HSF is an algebraic equation that is extensively used for adaptive gain variation in classical controllers because they are symmetrical, bounded, smooth, and differentiable (Saleem and Mahmood-ul-Hasan, 2018). The realization of this algebraic equation is computationally economical. Unlike gradient-descent based auto-tuning techniques, the nonlinear scaling functions do not put recursive computational burden on the embedded processor, and hence, they can be easily implemented via modern-day digital computers. The detailed formulation and benefits afforded by each adaptive reconfiguration approach are discussed as follows.

5.1. Pre-calibrated Reconfiguration Block

This reconfiguration block is used as baseline adaptive modulator to compare and verify the feasibility of the proposed scheme in effectively rejecting the influence of parametric uncertainties. This reconfiguration strategy adaptively modulates the value of ρ online in accordance with system's state-error dynamics.

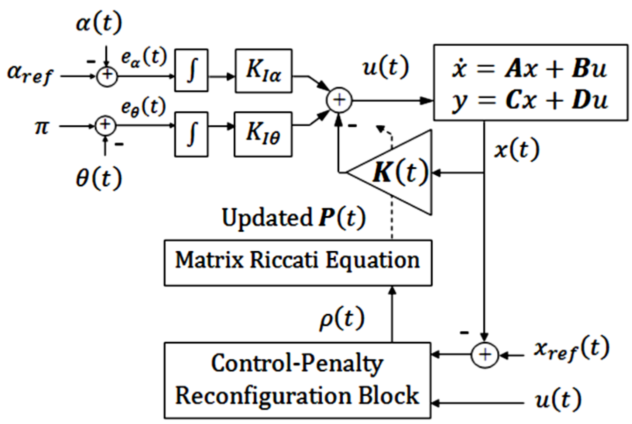

Fig. 2. Proposed adaptive control framework

The proposed algorithm undertakes to improve the system's response speed and damping strength against bounded exogenous perturbations, irrespective of the applied control effort. In under-actuated systems, the control resources contributed by the controller with fixed ρ may not be sufficient to overcome the detrimental effects rendered by large disturbances (Filip et al., 2019). Similarly, the control input resources contributed by the controller with fixed ρ may be unnecessarily excessive under low error conditions, rendering it wasteful in such conditions. In order to cope with such practical scenarios, the following rationale is suggested to reconfigure the value of ρ.

- The value of ρ is maintained at its nominal level for lower magnitudes of state-error variables. This arrangement allows for reference tracking with minimal control energy consumption.
- The value of ρ is depressed under high disturbance conditions; that is, when the magnitudes of state-error variables increase. This arrangement renders stronger damping control effort.

The aforementioned rules significantly enhance the disturbance-rejection capability. The impact of disturbance is measured by computing a linear sum of the state-error variables and their time-derivatives, as shown in (18).

$$g(t) = \mu_1 . e_\alpha(t) + \mu_2 . e_\theta(t) + \mu_3 . \dot{e}_\alpha(t) + \mu_4 . \dot{e}_\theta(t) \qquad (18)$$

where, $g(.)$ is the weighted sum of state-error variables and their time-derivatives. This expression is fed as the input to the HSF, expressed in (19), to reconfigure the value of ρ.

$$\rho(t) = \rho_{min} + (\rho_{max} - \rho_{min}). \mathrm{sech}(\beta_o . |g(t)|) \qquad (19)$$

where, $\mathrm{sech}(.)$ represents the HSF, ρ_{max} and ρ_{min} represent the upper and lower bounds of HSF, and β_o is the pre-fixed variation-rate of HSF. These hyper-parameters are empirically tuned a priori by minimizing J_e to attain strong damping against disturbances. The selected values are recorded in Table 2. This controller is denoted as Reconfigurable-LQR, or "RLQR", in this research.

5.2. Self-regulating Reconfiguration Block

The aforementioned strategy is sub-optimal. It applies tight control effort to efficiently reject the disturbances and damp the overshoots, while rendering large actuating torques in the control input (as shown in section 6).

Table 2. Parameter selection of pre-calibrated HSF

Parameter	Range	Tuned value
ρ_{max}	[0, 10]	1.04
ρ_{min}	[0, 10]	0.21
β_o	[0, 10]	8.15
μ_1	[0, 10]	0.78
μ_2	[0, 10]	2.25
μ_3	[0, 10]	0.26
μ_4	[0, 10]	0.69

The induction of peak servo requirements tends to saturate the actuator which eventually leads to complete de-stabilization of the RIP system. It is well-known that, in LQR problem, the enlargement of ρ limits the control input expenditure of the system under transient disturbance conditions at the cost of affecting its response-speed, and vice-versa (Lewis et al., 2012; Filip et al., 2019). This feature is beneficial in preventing the electro-mechanical system's actuator from getting saturated. Hence, this research work contributes to enhance the adaptability of the reconfiguration block by augmenting it with an original nonlinear-type self-regulating mechanism that is designed to deliver the following characteristics.

- The value of ρ is depressed under large disturbances to tighten the control effort, and vice-versa, as shown in expression (19).
- However, if the control-input tends to inflate significantly under exogenous disturbances, then the variation-rate of the $\rho(t)$ is reduced appropriately to soften the control effort and limit the magnitude of peak actuating torques.

This rationale uses the state-error and control-input variables simultaneously to modify the value of ρ. The proposed rationale is digitally realized by implanting the control-input variable as an additional input in the expression of $\rho(t)$, shown in (19). This auxiliary variable self-regulates the variation-rate of HSF waveform in real time. The proposed self-regulating HSF is shown below.

$$\rho(t) = \rho_{min} + (\rho_{max} - \rho_{min}). \mathrm{sech}(\, \beta(u,t). |g(t)| \,) \qquad (20)$$

$$\text{where,} \qquad \beta(u,t) = \beta_o . \left(\sigma + \frac{1-\sigma}{1 + |k. u(t)|^\gamma} \right)$$

where, σ is the positive constant that determines the minimum limit of variation-rate, k is the positive scaling factor of $u(t)$, γ is the positive fractional exponent of the magnitude of $u(t)$ that decides the dead-zone bandwidth to prevent self-regulation at lower value of control input. The parameters σ, k, and γ are tuned offline by iteratively minimizing J_e. The tuned values of these hyper-parameters are given in Table 3. The remaining parameters in the self-regulating HSF, in (20), are assigned the same values as prescribed earlier in Table 2. This augmentation dynamically alters (slows down) the variation-rate of HSF to limit the control energy consumption without significantly affecting the disturbance-rejection capability. The self-regulating property is useful when the control input profile exhibits large persistent fluctuations. The automatic adjustment rendered in the shape of HSF waveform, under large actuating torques, is depicted in Fig. 3.

Table 3. Parameter selection of self-regulating HSF

Parameter	Range	Tuned value
γ	[0, 10]	1.52
k	[0, 10]	0.08
σ	[0, 10]	0.25

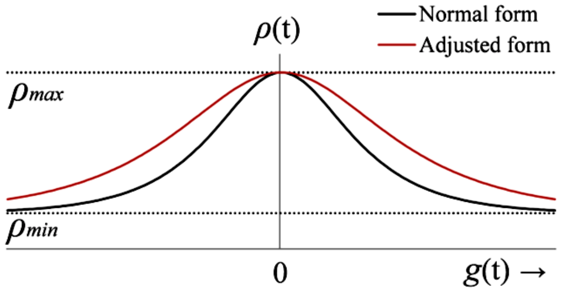

Fig. 3. Automatic adjustment in HSF waveform

The proposed self-regulating HSF increases the degree-of-freedom of the reconfiguration block by unifying the effects of variations in control-input and state-error dynamics in a single framework. This adaptive controller is denoted as Self-regulating Reconfigurable-LQR, or "SRLQR", in this paper.

6. EXPERIMENTS AND RESULTS

This section presents the experimental analysis procedure and the corresponding outcomes of each controller being tested.

6.1. Hardware setup

The QNET 2.0 Rotary Pendulum board is shown in Fig. 4 (Saleem and Mahmood-ul-Hasan, 2019). The variations in θ and α are measured by using the rotary encoders that are coupled with the rod and motor-shaft, respectively. The NI-ELVIS II data-acquisition board is used to digitize the encoder measurements at a sampling rate of 1000 Hz. The sampled data is serially transmitted at 9600 bps to the control software that is running on a 2.0 GHz, 6.0 GB RAM embedded computer. The control application is implemented in a virtual instrument file LabVIEW software by using its built-in "Block Diagram" tool.

Fig. 4. QNET 2.0 Rotary Pendulum board

The front-end of the control application is used as a graphical-user-interface to record and visualize the real-time state and control-input variations. The control software transmits the generated control signals to a motor driver circuit that is installed on the hardware setup. The motor driver transforms the incoming signals into pulse-width-modulated signals to actuate the DC motor. In this research, the clockwise rotation of the pendulum is considered as positive displacement. The pendulum rod is swung up and balanced manually at the beginning of every trial.

6.2. Experimental evaluation

The robustness of the SRLQR is compared with LQR and RLQR via "five" distinct hardware experiments. These test cases and their outcomes are presented as follows.

A. Position regulation: The reference-tracking accuracy of the pendulum is tested by allowing the arm to maintain its initial position with minimum deviations as the rod balances itself vertically under normal conditions. The time-domain profile of θ, α, V_m, and $\boldsymbol{K}(t)$ are shown in Fig. 5.

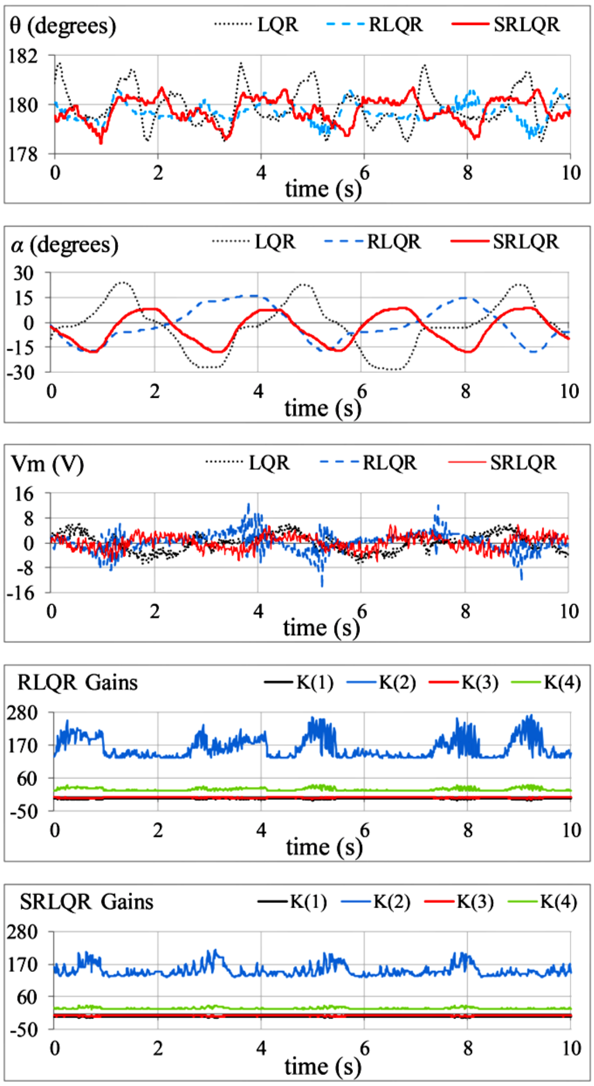

Fig. 5. Pendulum's response under normal conditions

B. Impulsive-disturbance rejection: The controller's ability to reject the impact of bounded impulsive exogenous disturbance(s) is tested by injecting a pulse signal directly in the system's control input (V_m). The injected signal has a magnitude of +5.0 V and time-duration of 0.1 s. The signal is artificially applied when the response of pendulum arm, α, of each controlled system approaches the second and third local maxima(s). The corresponding variations in θ, α, V_m, and $\boldsymbol{K}(t)$ are shown in Fig. 6.

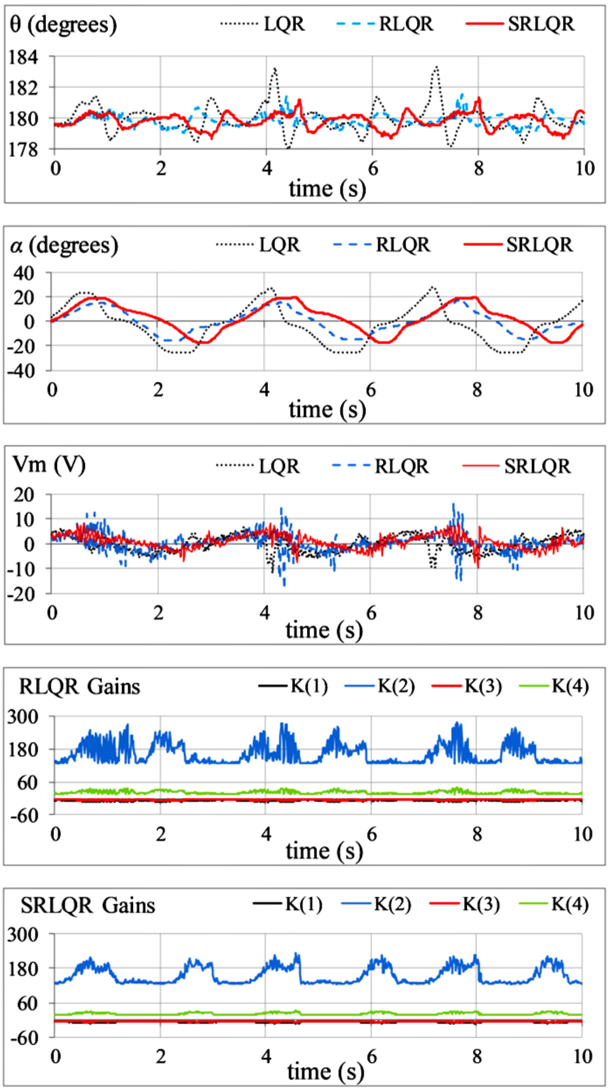

Fig. 6. Pendulum's response under impulsive disturbances

C. Step-disturbance attenuation: The controller's resilience to tolerate and compensate the effects of permanent load changes is examined by injecting a +5.0V step-signal in the control input (V_m) of the system at $t \approx 4.0$ s mark. This test case emulates the effects of applying exogenous torques on the system's body dynamics. The corresponding perturbations in θ, α, V_m, and $\boldsymbol{K}(t)$ are shown in Fig. 7.

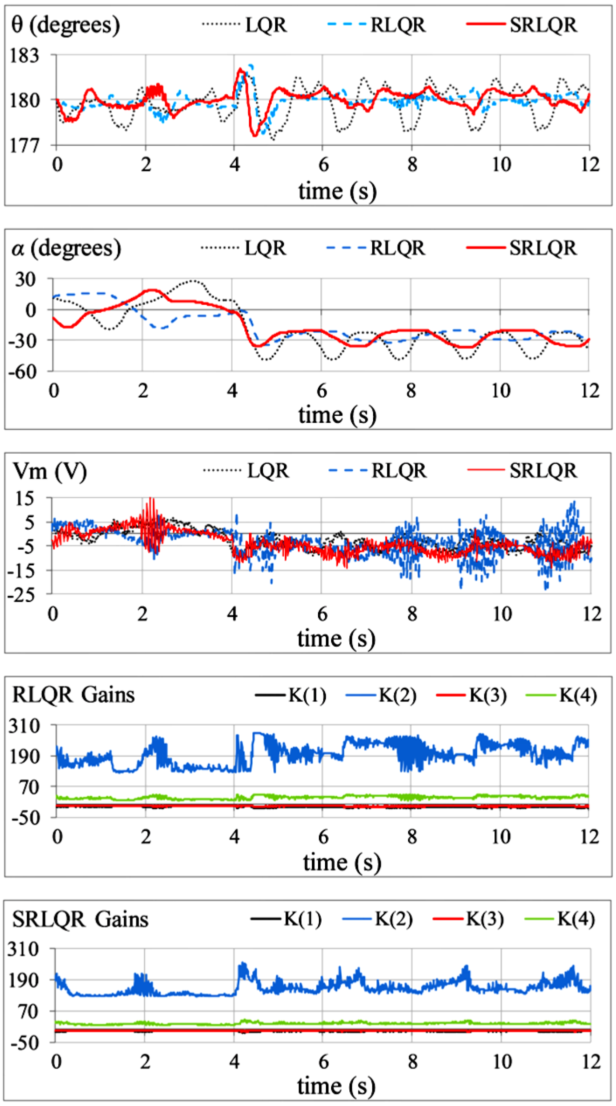

Fig. 7. Pendulum's response under step disturbance

D. Noise immunity: The system's position-regulation accuracy is also tested under the influence of process noise contributed by the parasitic impedances of electronic components, measurement noise of sensors, and mechanical vibrations. For this purpose, a low-amplitude and high-frequency sinusoidal signal, $d(t) = 1.5\sin(20\pi t)$, is injected in the reference input at $t \approx 0$ s. The corresponding variations in θ, α, V_m, and $\boldsymbol{K}(t)$ are shown in Fig. 8.

E. Modelling-error compensation: The controller's immunity against identification-errors and modeling-variations is examined by hooking up a 0.10 kg mass beneath the surface of pendulum's arm, as shown in Fig. 9, at $t \approx 4.0$ s mark. This modification permanently alters the coefficients of matrix $\boldsymbol{A}$ in the state-space model, and hence, disturbs the system's position-regulation behavior. The corresponding variations in θ, α, V_m, and $\boldsymbol{K}(t)$ are shown in Fig. 10.

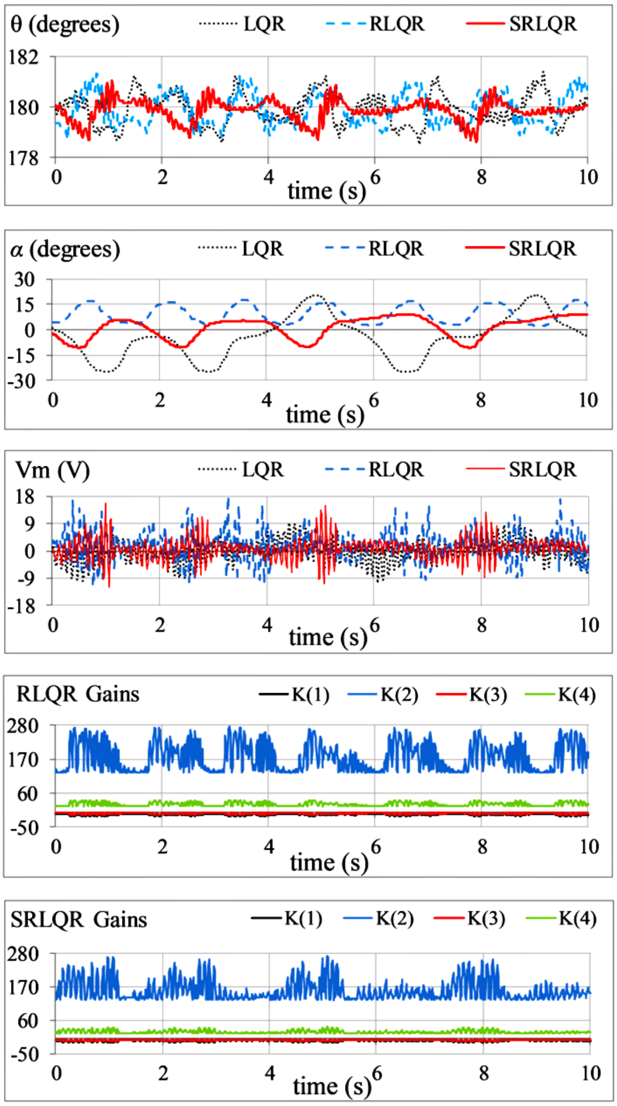

Fig. 8. Pendulum's response under sinusoidal noise signal

Fig. 9. Pendulum setup with 0.10 kg mass attached to arm

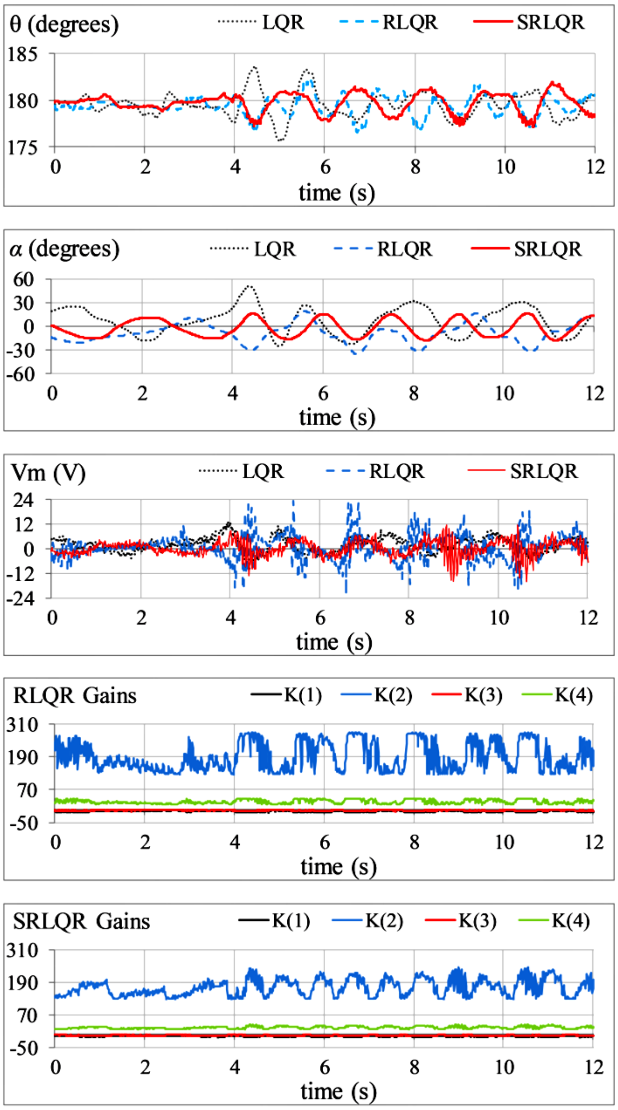

Fig. 10. Pendulum's response under modelling-error

5.3. Analytical discussion

The experimental results are analyzed on the basis of following Key-Performance-Indicators (KPIs).

- The time taken (t_s) by the response to settle within ±2% of the reference.
- The magnitude of overshoot and undershoot ($M_{p,x}$) in the response.
- The Root-Mean-Square-Error ($RMSE_x$) in the response.
- The offset error (E_{offset}) in arm's position under step-disturbance.
- The peak-to-peak magnitude of oscillations (α_{p-p}) in the arm's position under disturbances.
- The Mean-Square-Voltage (MSV) applied to DC motor. It is used as a measure of control-input energy.
- The magnitude of peak voltage spike (V_p) detected in the control profile.

The quantitative analysis of the graphical results, in terms of the aforementioned KPIs, is summarized in Table 4.

Table 4. Summary of experimental results

Test	KPI	Controllers		
		LQR	**RLQR**	**SRLQR**
A	$RMSE_\theta$ (deg.)	0.75	0.49	0.52
	$RMSE_\alpha$ (deg.)	14.90	10.38	9.55
	MSV (V^2)	8.32	11.02	6.82
B	$RMSE_\theta$ (deg.)	0.83	0.50	0.49
	$\lvert M_{p,\theta}\rvert$ (deg.)	3.34	1.58	1.19
	$t_{s,\theta}$ (s)	0.70	0.66	0.65
	$RMSE_\alpha$ (deg.)	15.88	9.88	10.44
	V_p (V)	11.88	17.93	9.79
	MSV (V^2)	10.61	12.92	8.65
C	$RMSE_\theta$ (deg.)	1.11	0.58	0.61
	$RMSE_\alpha$ (deg.)	28.72	22.59	22.62
	α_{p-p} (deg.)	26.25	11.77	14.45
	E_{offset} (deg.)	-32.83	-26.46	-26.47
	V_p (V)	10.73	24.49	12.42
	MSV (V^2)	19.65	37.30	21.08
D	$RMSE_\theta$ (deg.)	0.63	0.56	0.44
	$RMSE_\alpha$ (deg.)	13.21	9.93	6.36
	MSV (V^2)	12.25	23.09	11.31
E	$RMSE_\theta$ (deg.)	1.41	1.13	1.06
	$RMSE_\alpha$ (deg.)	18.84	13.44	11.06
	MSV (V^2)	16.23	37.43	18.15

In every test-case, the fixed-gain LQR demonstrates poor position-regulation behavior. The RLQR demonstrates significant enhancement in the time-domain response of α and θ as compared to the LQR. However, amid transient disturbances, the RLQR consumes considerably large control-input energy and exhibits peak actuating torques while rejecting the disturbances. The experimental results validate the improved robustness and control-input economy contributed by the proposed SRLQR. It exhibits rapid transits with improved damping strength against disturbances. It significantly minimizes the system's overall control-input expenditure as compared to RLQR. Furthermore, the control energy consumption of SRLQR is reasonably comparable with that of LQR. Apart from demonstrating optimum state and control behavior, the SRLQR also maintains the system's asymptotic-stability under every operating condition.

In Test-A, the SRLQR controlled system exhibits minimum RMSE in the time-domain response of *α*. The SRLQR controlled system shows 30.0% reduction and only 6.1% increment in $RMSE_\theta$ as compared to LQR and RLQR, respectively. The control-input energy utilized by SRLQR is approximately 42.1% and 56.2% lesser than the energy consumed by LQR and RLQR, respectively. In Test-B, the SRLQR exhibits minimum transient-recovery time to effectively attenuate the oscillations and shows minimum M_p in the time-domain profile of θ while compensating the impulsive disturbances. Apart from minimizing the overall control energy expenditure, it successfully limits the peak actuating voltage to 9.79 V, which is 45.4% lesser than that of RLQR. In Test-C, the SRLQR shows similar time-domain behavior as RLQR. It contributes slightly larger peak-to-peak oscillations in the response of *α*, as compared to RLQR, while damping the step-disturbance. However, the SRLQR consumes 34.6% lesser control energy than RLQR. It also brings down the V_p to almost one-half of that utilized by RQLR while damping the same disturbance. In Test-D, the SRLQR-controlled system precisely tracks the reference positions by contributing minimum RMSE and peak servo requirements. In Test-E, despite the disturbances caused by model variations, the SRLQR manages to balance the RIP system with minimum reference-tracking error. It successfully damps the state fluctuations, while consuming almost 46.4% lesser control-input energy than the RLQR.

7. CONCLUSION

This paper presents the formulation of a pragmatic indirect self-tuning strategy that enhances the robustness of adaptive state-feedback controllers for under-actuated electro-mechanical systems. The proposed self-tuning framework is synthesized by dynamically adjusting the control penalty-factor associated with controller's QPI. The control penalty-factor is adaptively modulated online via a state-error dependent self-regulating online adaptation mechanism. The experimental outcomes yielded by the proposed SRLQR are equated with the fixed-gain LQR and the baseline RLQR scheme to analyze the benefits afforded by it. The QNET 2.0 RIP system is used as the benchmark to conduct hardware experiments and comparatively assess the performance of each controller. The results clearly validate that the proposed SRLQR renders superior time-optimal behavior with reasonably good control economy. It significantly enhances the response speed and damping strength of the system against exogenous disturbances caused by environmental indeterminacies. There is a lot of room for future enhancements. Soft computing techniques, iterative learning schemes, and intelligent tuning mechanisms can be investigated for flexible online modulation of the control penalty-factor. The efficacy of the proposed adaptive control scheme can be further explored by using it to control other under-actuated mechatronic systems.

REFERENCES

An-chyau, H., Yung-feng, C., and Chen-yu, K. (2015). *Adaptive Control of Underactuated Mechanical Systems*. World Scientific, Singapore.

Basua, B., and Nagarajaiaha, S. (2008). A wavelet-based time-varying adaptive LQR algorithm for structural control. *Engineering Structures*, 30, pp. 2470–2477.

Batmani, Y., Davoodi, M., and Meskin, N. (2017). Nonlinear Suboptimal Tracking Controller Design Using State-Dependent Riccati Equation Technique. *IEEE Transactions on Control Systems Technology*, 25(5), pp. 1833-1839.

Bavili, R.E., Khosrowjerdi, M.J., Vatankhah, R. (2015). Active Fault Tolerant Controller Design using Model Predictive Control. *Control Engineering and Applied Informatics*, 17(3), pp. 68-76.

Bhatti, O.S., Mehmood-ul-Hasan, K., and Imtiaz, M.A.. (2015). Attitude Control and Stabilization of a Two-

Wheeled Self Balancing Robot. *Control Engineering and Applied Informatics*, 17(3), pp. 98-104.

Bhatti, O.S., Tariq, O.B., Manzar, A., and Khan O.A. (2018). Adaptive intelligent cascade control of a ball-riding robot for optimal balancing and station-keeping, *Advanced Robotics*, 32(2), pp. 63-76.

Boubaker, O., and Iriarte, R. (2017). *The Inverted Pendulum in Control Theory and Robotics: From Theory to New Innovations*. Institution of Engineering and Technology, Stevange, England.

Filip, I. and Szeidert, I. (2017). Tuning the control penalty factor of a minimum variance adaptive controller. *European Journal of Control*, 37, pp. 16-26.

Filip, I., Vasar, C., Szeidert, I., and Prostean, O. (2019). Self-tuning strategy for a minimum variance control system of a highly disturbed process. *European Journal of Control*, 46, pp. 49-62.

Filip, I., Dragan, F., Szeidert, I., and Albu, A. (2020). Minimum-Variance Control System with Variable Control Penalty Factor. *Applied Sciences*, 10(7), 2274, pp. 1-21.

Ghartemani, M.K., Khajehoddin, S.A., Jain, P., and Bakhshai, A. (2011). Linear quadratic output tracking and disturbance rejection. *International Journal of Control*, 84(8), pp. 1442-1449.

Kavuran, G., Ates, A., Alagoz, B.B., Yeroglu, C. (2017). An Experimental Study on Model Reference Adaptive Control of TRMS by Error-Modified Fractional Order MIT Rule. *Control Engineering and Applied Informatics*, 19(4), pp. 101-111.

Lewis, F.L., Vrabi,e D., and Syrmos, V.L. (2012). *Optimal Control*. John Wiley and Sons, New Jersey, USA.

Mahmoud, M. (2018). *Advanced Control Design with Application to Electromechanical Systems*. Elsevier Science, New York, pp. 177-253.

Nekoo, S.R., and Geranmehr, B. (2014). Nonlinear observer-based optimal control using the state-dependent Riccati equation for a class of non-affine control systems. *Control Engineering and Applied Informatics*, 16(2), pp. 5-13.

Ning, H., Zhang, J., Jing, X, and Tian, T. (2019). Robust Online Learning Method Based on Dynamical Linear Quadratic Regulator. *IEEE Access*, 7, pp. 117780-117795.

Önkol M, Kasnakoğlu C. Adaptive Model Predictive Control of a Two-wheeled Robot Manipulator with Varying Mass. Measurement and Control, 2018, 51(1-2), pp. 38-56.

Prasad, L.B., Tyagi, B., and Gupta, H.A. (2014). Optimal Control of Nonlinear Inverted Pendulum System Using PID Controller and LQR: Performance Analysis Without and With Disturbance Input. *International Journal of Automation and Computing*, 11(6), pp. 661–670.

Saleem, O., Hassan, H., Khan, A., and Javaid, U. (2017). Adaptive Fuzzy-PD Tracking Controller for Optimal Visual-Servoing of Wheeled Mobile Robots. *Control Engineering and Applied Informatics*, 19(3), pp. 58-68.

Saleem, O., Abbas, F., Khan, M.U., Imtiaz, M.A., and Khalid, S. (2018). Adaptive Collaborative Position Control of a Tendon-Driven Robotic Finger. *Control Engineering and Applied Informatics*, 20(2), pp. 87-99.

Saleem, O., Rizwan, M., and Ahmad, M. (2018). Augmented Linear Quadratic Tracker for Enhanced Output-Voltage Control of DC-DC Buck Converter. *Control Engineering and Applied Informatics*, 20(4), pp. 40-49.

Saleem, O., and Mahmood-ul-Hasan, K. (2018). Adaptive collaborative speed control of PMDC motor using hyperbolic secant functions and particle swarm optimization. *Turkish Journal of Electrical Engineering and Computer Sciences*, 26(3), pp. 1612-1622.

Saleem, O., and Rizwan, M. (2019). Performance optimization of LQR-based PID controller for DC-DC buck converter via iterative-learning-tuning of state-weighting matrix. *International Journal of Numerical Modelling*, 32(03), e2572, pp. 1-17.

Saleem, O., Rizwan, M., Shiokolas, P.S., Ali, B. (2019). Genetically Optimized ANFIS-based PID Controller Design for Posture-Stabilization of Self-Balancing-Robots under Depleting Battery Conditions. *Control Engineering and Applied Informatics*, 21(4), pp. 22-33.

Saleem, O., Shami, U.T., Mahmood-ul-Hasan, K., Abbas, F., and Mahmood, S. (2019). Robust-Optimal Output-Voltage Control of Buck Converter using Fuzzy Adaptive Weighted Combination of Linear Feedback Controllers. *Control Engineering and Applied Informatics*, 21(2), pp. 43-53.

Saleem, O., and Mahmood-ul-Hasan, K. (2019). Robust stabilisation of rotary inverted pendulum using intelligently optimised nonlinear self-adaptive dual fractional order PD controllers, *International Journal of Systems Science*, 50(7), pp. 1399-1414.

Saleem, O., Rizwan, M., Mahmood-ul-Hasan, K., and Ahmad, M. (2020). Performance Enhancement of Multivariable Model-Reference Optimal Adaptive Motor Speed Controller using Error-Dependent Hyperbolic Gain Functions. *Automatika*, 61(1), pp. 117-131.

Shahab, E., Nikoobin, A., Ghoddosian, A. (2017). Indirect-based Approach for Optimal Swing up and Stabilization of a Single Inverted Pendulum with Experimental Validation. *Control Engineering and Applied Informatics*, 19(4), pp. 61-71, 2017.

Szuster, M., and Hendzel, Z. (2017). *Intelligent Optimal Adaptive Control for Mechatronic Systems*. Springer, Berlin, Germany.

Ullah, S., Khan, Q., Mehmood, A., and Akmeliawati, R. (2019). Integral backstepping integral sliding mode control of underactuated nonlinear electromechanical systems. *Control Engineering and Applied Informatics*, 21(3), pp. 42-50, 2019

Yang, S., and Zheng, M. (2018). H∞ Fault-Tolerant Control for Dynamic Positioning Ships based on Sampled-data. *Control Engineering and Applied Informatics*, 20(4), pp. 32-39.

Zhang, H., Wang, J., and Lu, G. (2014). Self-organizing fuzzy optimal control for under-actuated systems. *Journal of Systems and Control Engineering*, 228(8), pp. 578-590.